**Aalborg Universitet**

AALBORG UNIVERSITY

# Current Harmonics from Single-Phase Grid-Connected Inverters

*Examination and Suppression*

Yang, Yongheng; Zhou, Keliang; Blaabjerg, Frede

*Published in:*
I E E E Journal of Emerging and Selected Topics in Power Electronics

*DOI (link to publication from Publisher):*
10.1109/JESTPE.2015.2504845

*Publication date:*
2016

*Document Version*
Accepted author manuscript, peer reviewed version

Link to publication from Aalborg University

*Citation for published version (APA):*
Yang, Y., Zhou, K., & Blaabjerg, F. (2016). Current Harmonics from Single-Phase Grid-Connected Inverters: Examination and Suppression. *I E E E Journal of Emerging and Selected Topics in Power Electronics*, *4*(1), 221-233. https://doi.org/10.1109/JESTPE.2015.2504845

**General rights**
Copyright and moral rights for the publications made accessible in the public portal are retained by the authors and/or other copyright owners and it is a condition of accessing publications that users recognise and abide by the legal requirements associated with these rights.

- Users may download and print one copy of any publication from the public portal for the purpose of private study or research.
- You may not further distribute the material or use it for any profit-making activity or commercial gain
- You may freely distribute the URL identifying the publication in the public portal -

**Take down policy**
If you believe that this document breaches copyright please contact us at vbn@aub.aau.dk providing details, and we will remove access to the work immediately and investigate your claim.

Downloaded from vbn.aau.dk on: December 05, 2025

# Current Harmonics from Single-Phase Grid-Connected Inverters – Examination and Suppression

Yongheng Yang, *Member, IEEE,* Keliang Zhou, *Senior Member, IEEE,* and Frede Blaabjerg, *Fellow, IEEE*

***Abstract*—Environmental conditions and operational modes may significantly impact the distortion level of the injected current from single-phase grid-connected inverter systems, such as photovoltaic (PV) inverters, which may operate in cloudy days with a maximum power point tracking, in a non-unity power factor, or in the low voltage ride through mode with reactive current injection. In this paper, the mechanism of the harmonic current injection from grid-connected single-phase inverter systems is thus explored, and the analysis is conducted on single-phase PV systems. In particular, the analysis is focused on the impacts of the power factor and the feed-in grid current level on the quality of the feed-in grid current from single-phase inverters. As a consequence, an internal model principle based high performance current control solution is tailor-made and developed for single-phase grid-connected systems to produce high quality currents in different operation conditions, where a design procedure is also provided. The developed current controller in this paper can achieve a minimum steady-state error while maintaining a relatively fast transient response, and also being feasible in other single-phase applications as a promising harmonic mitigation solution. Experiments on single-phase grid-connected systems have verified the correctness of the relevant analysis and also the effectiveness of the tailor-made control solution in terms of good harmonic mitigation.**

***Index Terms*—Harmonics, repetitive control (RC), resonant control, power quality, single-phase inverters, photovoltaic (PV) systems, low voltage ride-through, reactive power injection**

## I. Introduction

IT WAS reported by the European Photovoltaic Industry Association (EPIA) that the world's solar power capacity passed the 100 gigawatts (GW) mark for the first time in 2012 [1], and now it approaches to 180 GW in 2014 [2]. With an imperative demand of clean energy, it can be predicted that more photovoltaic (PV) systems will be installed in the future [3]. Such intensely increasing PV integration into the grid also challenges the availability, the power quality [4]–[7] and the emerging reliability of the entire PV system, as it is of high intermittency. Consequently, specific grid requirements/demands (e.g., IEEE Std 1547-2003 [8] and IEC Standard 61727 [9]) are expected to be strengthened to regulate the grid-connected PV systems, especially in terms of power quality and ancillary services [10]. In the future, the single-phase grid-connected PV system will be more active in different operation modes, provide Low Voltage Ride-Through (LVRT) capability in the presence of a grid fault, and be equipped with reactive power compensation functionality [10]–[12]. In that case, this operational mode might degrade the power quality with the risk of introducing resonances to the entire power system. As a consequence, the control system should be enhanced to maintain the power quality both under normal operation with Maximum Power Point Tracking (MPPT) and in other ancillary service mode (e.g., non-unity power factor) to meet the existing or upcoming grid codes/requirements [11]–[16].

For grid-connected inverter systems, including PV systems, the current distortion level is one important power quality index [17], [18]. For instance, it is stated in both the IEEE Std 1547-2003 and the IEC Standard 61727 that the Total Harmonic Distortion (THD) for the grid current should be lower than 5% to avoid adverse effects on other equipment that is connected to the grid [8], [9], [19], [20]. Moreover, for each individual odd harmonic from 3$^{rd}$ to 9$^{th}$, the limitation is 4% and at the same time the even harmonics are limited to 25% of the odd harmonic limits [8]. These acceptable current distortion levels are defined for grid-connected inverter systems (e.g., PV inverters) in the case of a rated output operational mode. However, taking the PV inverter systems as an example, due to the intermittency of solar irradiance, the output current of the PV inverter is usually less than its rated value. Furthermore, most PV inverters designed for grid-connected service operate close to unity power factor but in a partial loading condition. It is required that the PV system should operate at an average lagging power factor greater than 0.9 when the output power is greater than 50% of its rated power [9]. Beyond such basic requirements, the PV systems are expected more active in the future with reactive power compensation and fault ride through capability as aforementioned [12]. Although a pre-designed grid-connected PV system can meet the clauses in existing grid requirements, it is still not clear whether the current distortion level with non-unity power factor and/or the current level below its nominal value will make the system exceed the distortion level during operation or not. Obviously, the grid requirements have a strong impact on the design, performance, and operation of

Manuscript received May 17, 2015; revised October 8, 2015; accepted November 24, 2015. This is the peer-reviewed version of a paper accepted by IEEE Journal of Emerging and Selected Topics in Power Electronics. This work was under a SOLAR-ERA.NET transnational project [PV2.3 - PV2GRID] supported by the European Commission within the European Union's Seventh Framework Program (FP7/2007-2013). Recommended for publication by Associate Editor X. XX.

Y. Yang and F. Blaabjerg are with the Department of Energy Technology, Aalborg University, Aalborg 9220, Denmark (e-mail:yoy@et.aau.dk; fbl@et.aau.dk).

K. Zhou is with the Division of Systems, Power and Energy at the School of Engineering, University of Glasgow, Glasgow G12 8QQ, Scotland UK (e-mail: keliang.zhou@glasgow.ac.uk).

Color versions of one or more of the figures in this paper are available online at http://ieeexplore.ieee.org

Digital Object Identifier 10.1109/JESTPE.2015.2504845

Post-Print

the PV inverter systems. In order to guarantee a satisfactory current distortion level for grid-connected inverter systems in different operation modes, at least in the normal operation, these clauses in grid requirements have to be re-examined [10], [21], [22].

Control strategies that are applied to the power electronics converters could underpin the power conditioning functionality of the current and future grid-connected inverters [13]. In respect to the current control, a Proportional-Integral (PI) controller is the most popular controller for three-phase inverters because of its simplicity and the zero steady-state tracking error with the help of Park and Clark transformations. For single-phase inverter systems (e.g., PV inverters), a Proportional-Resonant (PR) controller [14], [23] is widely used, where a virtual orthogonal system should be developed. This actually can be transformed to the PI controller [24]. However, the PR controller can provide several advantages, such as much less computational burden and complexity due to its lack of Park transformations and simple to implement. Thus, the PR controller becomes a popular current regulator for grid-connected single-phase systems [13]–[15], [23], [25]–[31]. It is well known that odd harmonics (e.g., the 3$^{rd}$, 5$^{th}$ and 7$^{th}$) are dominant in the spectrum of the output current of single-phase grid-connected inverters. The PR controlled inverters may not be able to feed high quality currents into the grid, since a single PR controller cannot reject all harmonics appearing in the grid current.

In order to eliminate the current harmonic distortion effectively, Multi-Resonant Controllers (MRC) are plugged into the PR controller [13]–[15], [23], [25]. However, such a control scheme will increase the computational burden, particularly when high-order harmonics (e.g., 11$^{th}$ and 13$^{th}$) are required to be compensated. This might also trigger the system resonances, if the phase lead compensators are improperly designed. In contrast, a Repetitive Current (RC) controller with a simple phase compensator can track or reject all harmonics below the Nyquist frequency [19], [32]–[36], but it presents a much slower dynamic response than what a PR controller or a resonant controller does [37]–[40]. In order to suit power system specifications, high-performance control strategies should achieve a minimum steady-state error while maintaining a fast transient response, and also being feasible in practical implementations. To tackle these issues, a hybrid controller by combining the PR, the RC, and the MRC controllers is developed for a single-phase cascaded multi-level converter [41], [42]; a general parallel structure RC scheme is also introduced to multi-phase converters [40]. However, there is a still a gap to fill in on how to ensure single-phase grid-connected inverters (e.g., PV systems) to produce high quality currents in different operation modes. The root causes of harmonics from single-phase grid-connected inverter systems remain of high interest.

In light of the above considerations, the mechanism of the harmonic current injection from single-phase grid-connected inverter systems is presented in this paper, and the analysis is demonstrated on single-phase PV systems. In particular, for single-phase grid-connected PV systems in different operational modes, the impacts of the power factor and the output current level on the feed-in grid current distortion level are analyzed in details in § II. On the basis of the discussions, a high performance current control solution is developed for single-phase grid-connected inverter systems to produce high quality current in different operational modes. Moreover, essential design guidelines for the tailor-made controller have been provided in § III. Experiments on single-phase grid-connected systems are performed to examine the correctness of the relevant analysis and the effectiveness of the tailor-made control solution, and the results are given in § IV. Finally, § V draws the conclusion.

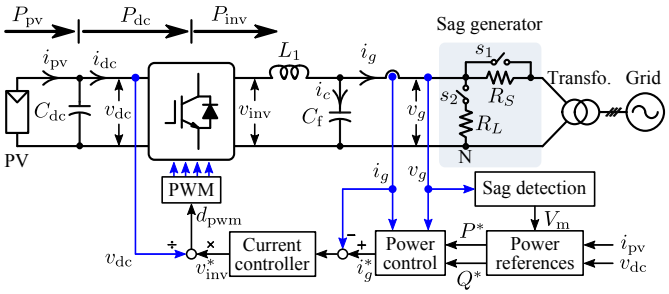


Fig. 1. Overall control structure of a single-phase single-stage grid-connected PV system based on the single-phase $PQ$ theory [43], which shows a simple voltage sag generator.

## II. Current Harmonic Injection Mechanism

In the following, the mechanism of harmonic injection from single-phase grid-connected inverter systems is demonstrated on a single-phase PV system. The discussion is mainly focused on how the input power (i.e., the feed-in current amplitude), the power factor, and the grid voltage amplitude will affect the current quality. Other origins of the harmonics such as the dead time effect, the non-linearity of power devices, and the grid background distortion are also commented on.

### A. Potentials of Current Quality Degradation

Fig. 1 shows a single-phase grid-connected PV system with a simple voltage sag generator, where the control is based on a single-phase $PQ$ theory [6], [15], [43], [44]. By adjusting the active power and reactive power references ($P^*$, $Q^*$), the power factor can be controlled. As aforementioned, the single-phase grid-connected PV system should fulfill the requirements/demands in different operational modes in such a manner to maintain the quality, the stability and the reliability of the entire system. Notably, those requirements tend to be even strengthened in the future, when the grid will become diverse and resilient. For instance, just like the case of wind power systems, the PV systems should be able to support the grid by means of injecting reactive current into the grid in the presence of a voltage drop [11], [12], [15], [22], [44]–[47]. Even in the normal operation mode, the grid voltage is not "constant" in terms of the amplitude. Furthermore, it should be pointed out that the future single-phase PV systems may also be required to provide ancillary services (e.g., Volt.-VAR control and $\cos\phi$-Watt control) [21], [48]–[52]. In that case, the power factor will not be unity, even when the PV system is

Post-Print

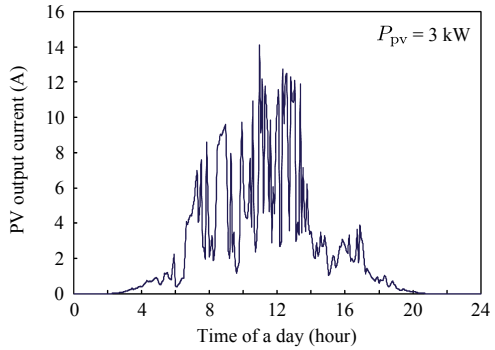


Fig. 2. Weather-dependency (i.e., intermittency) of the PV systems, indicating the effects on the output current and thus the injected grid current.

operating in the MPPT mode. Actually, since the PV inverters are normally under-designed, there is still room for the PV inverters to inject reactive power along with a MPPT control. In a word, the abnormal (or additional) operation in return can affect the current quality, e.g., LVRT operation and reactive power injection during nights [48], [49], and the power quality of PV inverters will possibly vary with the operational modes.

Additionally, in practice, the feed-in grid current level from a PV system will vary with the sites and the environmental conditions (as the intermittency, e.g., due to passing clouds in a cloudy day). Fig. 2 exemplifies the varying amplitude of the output current of a 3-kW PV system through a daily operation, which demonstrates the power fluctuations and the injected grid current variations of PV systems. Notably, this continuous injection of fluctuating power may be one of the potentials of grid current degradation, especially in the case of high penetration degree [53]. Nevertheless, the above scenarios can possibly affect the feed-in current quality. Since the design and operation modes of single-phase PV systems and thus the current quality will be impacted by the grid requirements/demands as discussed above, it calls for an investigation into the active clauses in existing grid requirements/demands and prompt the development of upcoming grid codes.

### *B. Current Harmonic Injection under Normal Conditions*

For the single-phase PV system shown in Fig. 1, it can be described by

$$\dot{i}_g = -C_{\rm f}\,\ddot{v}_g - \frac{1}{L_1}v_g + \frac{1}{L_1}v_{\rm inv} \tag{1}$$

and

$$\dot{v}_{\rm dc} = \frac{1}{C_{\rm dc}}(i_{\rm pv} - i_{\rm dc}) \tag{2}$$

where $v_{\rm inv}$ is the PV inverter output voltage, $v_g$ is the grid voltage, and $L_1$, $C_{\rm f}$ are the inductor and the capacitor of an inductor-capacitor (LC) filter, respectively. Since the filter capacitor $C_{\rm f}$ is used mainly to filter out the high frequency switching harmonics, Eq. (1) can be simplified as

$$\dot{i}_g = \frac{1}{L_1}(v_{\rm inv} - v_g) \tag{3}$$

when only considering the low-order harmonics. As a consequence, if the inverter output voltage $v_{\rm inv}$ and/or the grid voltage $v_g$ contain any low-order harmonics (referred to as background distortions), the injected grid current $i_g$ will be distorted, thus resulting in a poor $\text{THD}_{i_g}$. In that case, the grid current $i_g$ can be further written as

$$\begin{aligned} i_g &= \frac{1}{L_1}\int\left[\left(v_{\rm inv}^1 + \sum_{h=2}^{n} v_{\rm inv}^h\right) - \left(v_g^1 + \sum_{h=2}^{n} v_g^h\right)\right] \\ &= \underbrace{\frac{1}{L_1}\int\left(v_{\rm inv}^1 - v_g^1\right)}_{i_g^1} + \sum_{h=2}^{n} i_{g,\rm C}^h - \sum_{h=2}^{n} i_{g,\rm G}^h \end{aligned} \tag{4}$$

with

$$i_{g,\rm C}^h = \frac{1}{L_1}\int v_{\rm inv}^h, \text{ and } i_{g,\rm G}^h = \frac{1}{L_1}\int v_g^h \tag{5}$$

being the grid current harmonics induced by the inverter voltage harmonics $v_{\rm inv}^h$ and the grid voltage distortions $v_g^h$, respectively, $i_g^1$, $v_{\rm inv}^1$, and $v_g^1$ representing the fundamental components of the injected grid current, the inverter output voltage, and the grid voltage, and $h$ being the harmonic order.

It should be pointed out that the grid voltage distortions are normally uncontrolled, which are mainly induced by the non-linear loads that are connected to the grid. Fortunately, it is implied in (4) that the current harmonics (i.e., $\sum_{h=2}^{n} i_{g,\rm G}^h$) induced by the grid voltage distortions can be eliminated by the controllable inverter output voltage $v_{\rm inv}$ if a proper control method and/or modulation technique is applied to the grid-connected inverter. In such a control scheme, the inverter output voltage should consist of appropriate harmonic contents that can theoretically cancel out the harmonics induced by the grid voltage (i.e., $\sum_{h=2}^{n} v_g^h = \sum_{h=2}^{n} v_{\rm inv}^h$) in accordance to (4). The following thus analyses how the inverter output voltage harmonics are generated, which in return affects the feed-in grid current quality seen from (4) and (5).

On an assumption that the quality of the grid voltage is high (i.e., $v_g^h \approx 0$), the feed-in grid current harmonics induced by the grid voltage background distortions can thus be neglected (i.e., $\sum_{h=2}^{n} v_g^h \approx 0$). In that case, the harmonics induced by the inverter output voltage will dominate in the injected current, since a Pulse Width Modulation (PWM) scheme is typically applied to realize the DC-AC inversion using non-linear power semiconductors. Thus, it is reasonable to firstly conduct the harmonic analysis only in the consideration of $\sum_{h=2}^{n} i_{g,\rm C}^h$ shown in (4). In general, the inverter output voltage $v_{\rm inv}$ can be expressed as

$$\begin{aligned} v_{\rm inv} &= d_{\rm pwm} v_{\rm dc} = \left(d_{\rm pwm}^1 + \sum_{h=2}^{n} d_{\rm pwm}^h\right)\left(V_{\rm dc} + \tilde{v}_{\rm dc}\right) \\ &= d_{\rm pwm}^1 V_{\rm dc} + d_{\rm pwm}^1 \tilde{v}_{\rm dc} + V_{\rm dc}\sum_{h=2}^{n} d_{\rm pwm}^h + \tilde{v}_{\rm dc}\sum_{h=2}^{n} d_{\rm pwm}^h \\ &= v_{\rm inv}^1 + \sum_{h=2}^{n} v_{\rm inv}^h \end{aligned} \tag{6}$$

where $d_{\rm pwm}$ is the PWM signal with $-1 \le d_{\rm pwm} \le 1$ and $d_{\rm pwm}^1$, $d_{\rm pwm}^h$ being the fundamental component and harmonics of $d_{\rm pwm}$, respectively, $V_{\rm dc}$ and $\tilde{v}_{\rm dc}$ are the DC and AC components of the voltage $v_{\rm dc}$ across the DC-link capacitor $C_{\rm dc}$ shown in Fig. 1 (i.e., the dc-link voltage).

It is demonstrated by (6) that the inverter output voltage $v_{\rm inv}$ consists of a fundamental component $v_{\rm inv}^1$ and harmonics

Post Print

$v_{\text{inv}}^h$ that are induced by the PWM harmonics, $\sum_{h=2}^{n} d_{\text{pwm}}^h$, and the DC-link voltage variations, $\tilde{v}_{\text{dc}}$. As a consequence, the injected current will inevitably inherit the harmonics, and thus the power quality will be affected according to (4). Moreover, it can also be observed in (6) that $V_{\text{dc}} \sum_{h=2}^{n} d_{\text{pwm}}^h$ can possibly be utilized to eliminate the harmonics caused by $d_{\text{pwm}}^1 \tilde{v}_{\text{dc}}$ if the inverter controller is appropriately designed; otherwise $V_{\text{dc}} \sum_{h=2}^{n} d_{\text{pwm}}^h$ will even deteriorate the quality of the injected grid current. Here, the high-order term $\tilde{v}_{\text{dc}} \sum_{h=2}^{n} d_{\text{pwm}}^h$ is ignored, since it can be filtered out by the LC-filter and also for simplicity. The above analysis has revealed that the inverter output voltage will affect the grid current quality. Specifically, the grid current distortions are partially induced by a) the inverter PWM control applied to the inverter and b) the DC-link voltage variations.

Theoretically, the PWM harmonics, i.e., $\sum_{h=2}^{n} d_{\text{pwm}}^h$, are side-bands centered around the switching frequency and its multiples [54]. However, in practical applications, there are dead-time and non-linear turn-on (and turn-off) delays, which will contribute to low-order harmonic distortions [54]–[56], leading to degradation in the current quality according to (5) and (6). As for the DC-link voltage variations, prior-art study has shown that the DC-link voltage typically contains a double grid frequency component [13], [57]. In the following, an analysis on the DC-link voltage variations is carried out in order to give a better understanding of the current harmonic injection from single-phase inverters. Let us consider the fundamental grid voltage $v_g^1 = \sqrt{2}V_g^1 \cos(\omega_0 t + \varphi)$, the fundamental grid current $i_g^1 = \sqrt{2}I_g^1 \cos(\omega_0 t)$, and the inverter output voltage $v_{\text{inv}}^1 = \sqrt{2}V_{\text{inv}}^1 \cos(\omega_0 t + \varphi - \varphi_1)$ for the following discussion with $\omega_0$ and $\varphi$ being the grid fundamental angular frequency and the power angle, respectively. According to Fig. 1, the DC side instantaneous power $p_{\text{dc}}$ (i.e., the inverter input power) and the inverter output instantaneous power $p_{\text{inv}}$ can be obtained, respectively, as

$$\begin{aligned} p_{\text{dc}} &= v_{\text{dc}} i_{\text{pv}} - v_{\text{dc}} C_{\text{dc}} \frac{dv_{\text{dc}}}{dt} \\ &= v_{\text{dc}} i_{\text{pv}} - C_{\text{dc}} V_{\text{dc}} \frac{d\tilde{v}_{\text{dc}}}{dt} - C_{\text{dc}} \tilde{v}_{\text{dc}} \frac{d\tilde{v}_{\text{dc}}}{dt} \end{aligned} \tag{7}$$

$$\begin{aligned} p_{\text{inv}} = {} & V_{\text{inv}}^1 I_g^1 \cos(\varphi - \varphi_1) + V_{\text{inv}}^1 I_g^1 \cos(2\omega_0 t + \varphi - \varphi_1) \\ & + \left( i_g^1 \sum_{h=2}^{n} v_{\text{inv}}^h + v_{\text{inv}}^1 \sum_{h=2}^{n} i_g^h \right) \end{aligned} \tag{8}$$

where $i_g^h = i_{g,\text{C}}^h + i_{g,\text{G}}^h$ represents the total grid current harmonics. Neglecting the inverter losses and the losses on the DC-link capacitor $C_{\text{dc}}$ gives $p_{\text{inv}} = p_{\text{dc}}$ and also $p_{\text{pv}} = v_{\text{dc}} i_{\text{pv}} \approx V_{\text{inv}}^1 I_g^1 \cos(\varphi - \varphi_1)$. This also indicates that the DC-link capacitor is used for power decoupling and thus to handle the power variations between the DC side and the AC side, leading to the voltage variations. In most cases, since $|V_{\text{dc}}| \gg |\tilde{v}_{\text{dc}}|$, $|I_g^1| \gg |i_g^h|$, and $|V_{\text{inv}}^1| \gg |v_{\text{inv}}^h|$ and the high-order term $\tilde{v}_{\text{dc}} d\tilde{v}_{\text{dc}}/dt$ in the DC side instantaneous power $p_{\text{dc}}$ is ignored, the following is valid according to (7) and (8)

$$\tilde{v}_{\text{dc}} \approx -\int \left[ \frac{V_{\text{inv}}^1 I_{\text{g}}^1}{C_{\text{dc}} V_{\text{dc}}} \cos(2\omega_0 t + \varphi - \varphi_1) \right] dt \tag{9}$$

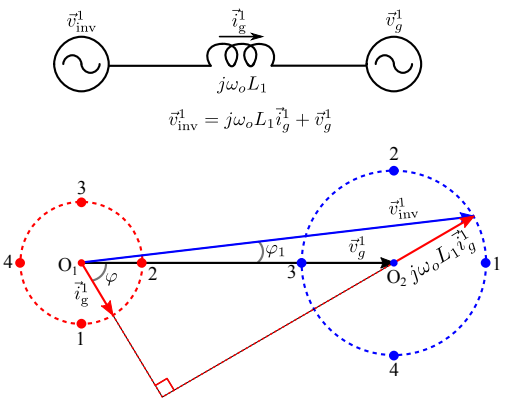


Fig. 3. Simplified model and the fundamental-frequency phasor diagram of the AC side circuit (LC-filter) shown in Fig. 1 with a lagging power factor.

which confirms that the DC-link voltage has a variation of twice the grid frequency.

Eq. (9) implies that the variation amplitude of DC bus voltage $|\tilde{v}_{\text{dc}}|$ is proportional to the fundamental amplitude of the inverter output voltage $V_{\text{inv}}^1$ and fundamental amplitude of the grid current $I_g^1$. In contrast, the variation amplitude is inversely proportional to the DC-link capacitor $C_{\text{dc}}$ and the DC-link voltage $V_{\text{dc}}$ [57]. The impact can also be further illustrated by the phasor diagram depicted in Fig. 3, which shows that the length of the inverter output voltage $\vec{v}_{\text{inv}}$ varies with the power angle. As a consequence, the larger the power angle (with 90°) is, and the larger the variation $|\tilde{v}_{\text{dc}}|$ will be. According to (4)-(6), it can be concluded that the variation $|\tilde{v}_{\text{dc}}|$ will introduce harmonics in the inverter output voltage $v_{\text{inv}}$. Moreover, it is shown in (9) that $\tilde{v}_{\text{dc}}$ mainly contains even harmonics with a double grid frequency, $2\omega_0$. Consequently, $d_{\text{pwm}}^1 \tilde{v}_{\text{dc}}$ will produce odd harmonics with the frequency of $(2k+1)\omega_0$, $k$ =1, 2, 3, $\cdots$. As a result, odd current harmonics will be injected by single-phase PV inverters because both $d_{\text{pwm}}^1$ and $\tilde{v}_{\text{dc}}$ are inevitable elements in a closed-loop control for a grid-connected inverter shown in Fig. 1.

In a word, the $\text{THD}_{i_g}$ of the feed-in current will be varying under a) different power factors (or $\cos\varphi$), which could happen in reactive power compensation periods, and b) different feed-in current levels, $I_g^1$. Although a single-phase system can meet the requirements in some cases, the current distortion level cannot always be maintained at a satisfied level even in normal operation conditions because of the changing environmental conditions (cf., Fig. 2) and operational modes according to the above discussions.

### C. Current Harmonic Injection under Voltage Sags/Swells

Several events like lightning and cable short-circuiting can cause grid faults, which will result in the variation of grid voltage or frequency, the change of the grid impedance, and possibly the absence of the utility grid, which represents an islanding operational mode. Subsequently, the grid voltage and/or frequency may excursion above or below the nominal values. In such cases, the PV systems are required to cease energizing for safety concerns. However, those grid requirements will become more stringent because of the still

Post-Print

increasing penetration of PV systems [21], [22], [48], where the PV inverters should remain connected under voltage faults. When ignoring the power losses on the filter, the instantaneous inverter output power $p_{\text{inv}}$ can also be expressed as

$$\begin{aligned} p_{\text{inv}} &= \left(v_g + L_1 \frac{di_g}{dt}\right) i_g \\ &= V_g^1 I_g^1 \cos\varphi + V_g^1 I_g^1 \cos\left(2\omega_0 t + \varphi\right) \\ &\quad -\omega_0 L_1 (I_g^1)^2 \sin\left(2\omega_0 t\right) + O(h) \end{aligned} \tag{10}$$

where the current through the capacitor of an LC-filter is also neglected and $O(h)$ represents the high order components, being

$$O(h)=\left(v_g^1+L_1\sum_{h=2}^{n}\frac{di_g^h}{dt}\right)\sum_{h=2}^{n} i_g^h + L_1\left(i_g^1+\sum_{h=2}^{n} i_g^h\right)\sum_{h=2}^{n}\frac{di_g^h}{dt}.$$

Similarly, ignoring the inverter power losses and the higher order components $O(h)$ gives

$$\tilde{v}_{\text{dc}} \approx -\int\left[\frac{V_g^1 I_g^1}{C_{\text{dc}} V_{\text{dc}}}\cos\left(2\omega_0 t+\varphi\right) - \frac{\omega_0 L_1 (I_g^1)^2}{C_{\text{dc}} V_{\text{dc}}}\sin\left(2\omega_0 t\right)\right] dt \tag{11}$$

which implies that the voltage variation $|\tilde{v}_{\text{dc}}|$ across the DC capacitor is proportional to the grid voltage amplitude $V_g^1$. Therefore, in the case of a voltage sag, the DC-link voltage variation is smaller if the grid current amplitude remains the same; while for voltage swells, the DC-link voltage variation becomes larger. Based on the phasor diagrams shown in Fig. 4, it can be predicted that the power quality will be better in the LVRT operation mode if the grid current level is kept the same, which can also ensure a stable LVRT operation without triggering the over-current protection [44]. In contrast, the high voltage ride through operation may result in a poor current quality according to (5) and (6) due to the increase of DC-link voltage variations. However, it should be noted that the first priority under voltage faults is focused on riding-through to stabilize the entire system. Thus, it is unnecessary to specify current quality in such cases. Nevertheless, this has revealed that the grid voltage (amplitude) variations will affect the injected current quality.

### *D. Other Origins for Current Harmonics*

The basic mechanism of harmonic current injection from a single-phase system has been elaborated above, where the grid voltage quality is assumed to be good enough. However, it should be noted that the grid voltage distortion will definitely affect the current quality according to (4). Moreover, the grid synchronization scheme, taking the grid voltage as input, is inevitable for single-phase systems. Thus, the performance of synchronization method might have an impact on the current quality [58]. For a specific case of PV systems, anti-islanding algorithms are required [14]. Among various islanding detection techniques, the active methods produce non-sinusoidal current reference ($i_g^*$, i.e., contains harmonics). Hence, according to Fig. 1, the inverter output voltage reference $v_{\text{inv}}^*$ will also be distorted (and thus the PWM signals $d_{\text{pwm}}$). It means that the anti-islanding algorithms for PV systems will also

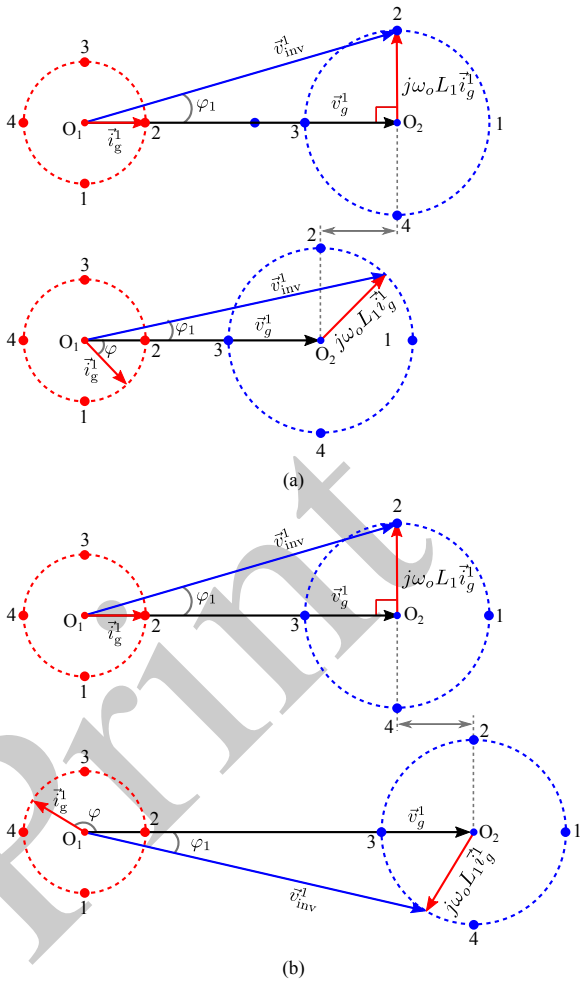


Fig. 4. Fundamental-frequency phasor diagrams for a single-phase grid-connected system in the case of (a) a voltage sag and (b) a voltage swell.

deteriorate the feed-in current to some extent. However, the current controller with harmonic compensators will alleviate this impact. As a result, the degradation in the feed-in current quality due to anti-islanding algorithms can be neglected.

Additionally, the previous discussion is done on the basis of a constant grid frequency (i.e., $\omega_0 = const.$). However, in practice, the grid frequency can not always be maintained as constant [59]. There might be frequency variations due to e.g. a continuous injection of a large amount of fluctuating renewable power. Such frequency variations may deteriorate the injected current quality and it can also cause instability for frequency-sensitive control systems [59], [60], such as resonant and repetitive control systems, especially implemented in the digital signal processors.

In different applications, the grid-connected inverter systems will operate in various sites and daily changing environmental conditions. Accordingly, the changing solar irradiance will directly affect the PV panel output power. As a result, the injected current level is affected and also the power quality will change, as discussed in § II. Thus, it is desirable to develop a high-performance current control solution for grid-connected single-phase PV systems to produce a high quality current regardless of the challenging conditions. That is to say, the

Post-Print

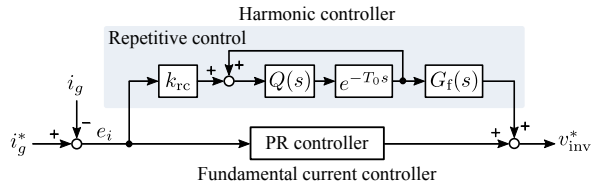


Fig. 5. Proportional resonant current controller with a repetitive based harmonic controller for the single-phase grid-connected systems.

preferred control method should not be sensitive to the changes of the power factor and/or the output current level.

## III. Current Harmonic Control

### A. Tailor-Made Control Solution

As it is shown in Fig. 1, if the current reference $i_g^*$ is a purely sinusoidal signal with a frequency of $\omega_0$ and at the same time the gains of the current controller at the harmonic frequencies are high enough, the injected grid current will be almost harmonic-free in the steady-state. Based on the above analysis, a Proportional Resonant (PR) [14], [23], [25]–[31], [61] plus Repetitive Current (RC) [19], [32]–[42], [62]–[67] controller is developed in order to eliminate the harmonic current injection under different conditions (e.g., non-unity power factor), as it is shown in Fig. 5. This current control scheme is designed to suppress the harmonic distortions caused by the DC-link voltage variations $d_{\text{pwm}}^1 \tilde{v}_{\text{dc}}$, the non-linearity of the power devices, the dead-time harmonics [55], and the grid voltage background distortions $\sum_{h=2}^{n} v_g^h$.

However, it should be noted that, although the RC can suppress all harmonics below the Nyquist frequency in theory, its dynamic response is very slow in removing high-order harmonics due to its fundamental period time-delay in the implementation. In contrast, the MRC, which connects the resonant controllers in parallel for the harmonics of interest, can eliminate selective harmonic distortions at a much faster speed [13], [14], [30], [31]. Yet, it is at the expense of heavy paralleling computation duty [68]. Moreover, as discussed previously, when higher order harmonics (above the 11th and/or 13th harmonics) need to be compensated, the MRC method is apt to cause the system to become unstable and it is less practical [38], [39], where multiple phase compensators are required accordingly. However, the developed current controller consists of a PR controller that is designed as a zero-tracking-error controller at the grid fundamental frequency and a RC controller that is designed to remove the harmonic components [41], [42]. As a consequence, combining the PR and RC controllers shown in Fig. 5 takes the strength of both controllers – fast tracking of the fundamental current and almost complete harmonic mitigation. It thus can make an optimal trade-off between control performance and practical realization.

### B. Design of the Current Controller

A Classic Repetitive Controller (CRC) can be given as

$$G_{\text{crc}}(s) = k_{\text{rc}} \frac{e^{-T_0 s}}{1 - e^{-T_0 s}} \tag{12}$$

where $k_{\text{rc}}$ is the control gain and $T_0$ is the fundamental period of the grid voltage with $\omega_0 = 2\pi/T_0$. Eq. (12) is expanded as

$$G_{\text{crc}}(s) = k_{\text{rc}} \left\{ -\frac{1}{2} + \frac{1}{T_0} \left[ \frac{1}{s} + \frac{2s}{s^2+\omega_0^2} + \sum_{h=2}^{\infty} \frac{2s}{s^2+(h\omega_0)^2} \right] \right\} \tag{13}$$

which indicates that the CRC is equivalent to a parallel configuration of a proportional controller (i.e., $-k_{\text{rc}}/2$), an integrator (i.e., $k_{\text{rc}}/(T_0 s)$) and infinite parallel-resonant controllers with an identical control gain, $2k_{\text{rc}}/T_0$. This MRC can be given as

$$G_{\text{mrc}}(s) = \frac{2k_{\text{rc}}}{T_0} \sum_{h=2}^{\infty} \frac{s}{s^2 + (h\omega_0)^2} \tag{14}$$

with $h$ being the harmonic order and $\omega_0$ being the fundamental grid angular frequency. As observed in (13) and (14), since the control gain for the MRC is identical, it is not possible for the CRC controller to eliminate selective harmonics effectively. That is to say, it is difficult for the CRC to optimally cancel out the harmonics of interest when compared to the MRC that acts on individual harmonics [59].

Considering the robustness of the CRC controller, a low-pass filter $Q(s)$ and a phase-lead compensator $G_{\text{f}}(s)$ are incorporated as shown in Fig. 5. Accordingly, the resultant RC controller, $G_{\text{rc}}(s)$ and the PR controller, $G_{\text{pr}}(s)$ shown in Fig. 5 can respectively be given as

$$G_{\text{rc}}(s) = k_{\text{rc}} \frac{e^{-T_0 s} Q(s)}{1 - e^{-T_0 s} Q(s)} \cdot G_{\text{f}}(s) \tag{15}$$

and

$$G_{\text{pr}}(s) = k_p + k_r \frac{s}{s^2 + \omega_0^2} \tag{16}$$

where $k_p$ and $k_r$ are the control gains for the PR controller, and $G_{\text{f}}(s) = e^{Ts}$ [38], [39], [62] with $T$ being the period of the phase-lead compensator. Since those current controllers are normally implemented in low-cost digital signal processors, it is more convenient to give their digital forms in the $z$-domain:

$$G_{\text{rc}}(z) = k_{\text{rc}} \frac{z^{-N} Q(z)}{1 - z^{-N} Q(z)} \cdot G_{\text{f}}(z) \tag{17}$$

and

$$G_{\text{pr}}(z) = k_p + k_r \cdot \frac{\sin(\omega_0 T_s)}{2\omega_0} \cdot \frac{1 - z^{-2}}{1 - 2\cos(\omega_0 T_s) z^{-1} + z^{-2}} \tag{18}$$

in which $N = f_s/f_0$ with $f_s$ being the sampling frequency and $f_0 = 1/T_0$ being the grid fundamental frequency, $T_s = 1/f_s$ is the sampling period, and the pre-warped bilinear (Tustin) transformation [23], [26], [29] has been used to discretize the PR controller of (16). $Q(z)$ and $G_{\text{f}}(z)$ are the transfer functions of the low-pass filter and the phase-lead compensator in the $z$-domain, respectively.

Based on Fig. 5 and the entire current control loop shown in Fig. 6, the closed-loop transfer function of the grid current $G_{\text{cl}}(z)$ can be obtained as

$$G_{\text{cl}}(z) = \frac{i_g(z)}{i_g^*(z)} = \frac{z^{-1} \left[ G_{\text{pr}}(z) + G_{\text{rc}}(z) \right] F(z)}{1 + z^{-1} \left[ G_{\text{pr}}(z) + G_{\text{rc}}(z) \right] F(z)} \tag{19}$$

where $z^{-1}$ represents the processing and PWM delay [69], [70], $F(z)$ is the transfer function of the inductor of the LC

Post-Print

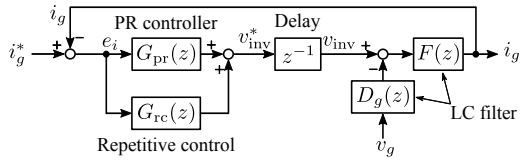


Fig. 6. Current control loop with the tailor-made current harmonic controller (a proportional resonant controller with a plug-in repetitive controller).

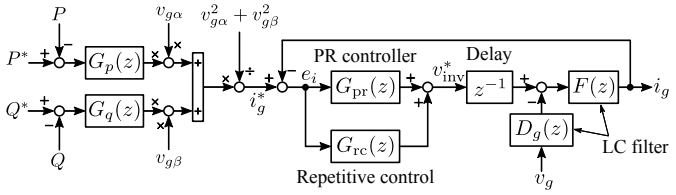


Fig. 7. Control scheme for a single-phase grid-connected system based on the single-phase $PQ$ theory [15], [43], [44] and the tailor-made current harmonics suppression method.

filter, and it is discretized as follows by means of bilinear transformation:

$$F(z) = \frac{T_s}{2L_1} \cdot \frac{1+z^{-1}}{1-z^{-1}}. \tag{20}$$

It should be mentioned that in the digital controlled PWM converters the delay time is normally taken as 1 to 1.5 times of the sampling period (i.e., $T_s$) [31], [69]. In this paper, a delay of $T_s$ corresponding to $z^{-1}$ is chosen for simplicity while maintaining a relatively high accuracy [69], [70]. Subsequently, the transfer function of the current tracking error $e_i(z) = i_g^*(z) - i_g(z)$ to the current reference can be described by

$$G_{\rm ei}(z) = \frac{e_i(z)}{i_g^*(z)} = \frac{1 - G_{\rm clPR}(z)}{1 + z^{-1}G_{\rm rc}(z)F(z)[1 - G_{\rm clPR}(z)]} \tag{21}$$

with $G_{\rm clPR}(z)$ being the current closed-loop transfer function only using the PR controller which can be given by

$$G_{\rm clPR}(z) = \frac{z^{-1}G_{\rm pr}(z)F(z)}{1 + z^{-1}G_{\rm pr}(z)F(z)}. \tag{22}$$

Hereafter, according to Fig. 1 and the single-phase $PQ$ theory, the closed-loop control scheme can be constructed as shown in Fig. 7, where $G_p(z)$, $G_q(z)$ are the PI controllers in the digital forms for the active power and reactive power, respectively, and $v_{g\alpha}$, $v_{g\beta}$ are the $\alpha\beta$ components of the grid voltage generated by a second-order generalized integrator based orthogonal generation system [13]–[15]. It should be pointed out that the control solution shown in Fig. 7 can ensure a proper power injection from the grid-connected inverter system in response to the grid conditions (e.g., voltage sag and reactive power injection) by setting the power references. Moreover, in order to improve the system dynamics, the two PI controllers can be removed [71], where there is no need for power calculation. The system parameters for the following discussion are listed in Table I.

TABLE I
PARAMETERS OF THE SINGLE-PHASE SINGLE-STAGE INVERTER SYSTEM (REFERRING TO FIG. 1).

| Parameter | Symbol | Value |
|---|---|---|
| Rated active power | $P_n$ | 1 kW |
| Grid voltage amplitude | $V_g$ | 325 V |
| DC-link voltage | $V_{\rm dc}$ | 400 V |
| DC-link capacitor | $C_{\rm dc}$ | 1100 $\mu$F |
| Grid frequency | $\omega_0$ | $2\pi \times 50$ rad/s |
| LC filter | $L_1$ | 3.6 mH |
| | $C_f$ | 2.35 $\mu$F |
| Transformer leakage inductance | $L_g$ | 4 mH |
| Sampling frequency | $f_s$ | 10 kHz |
| Switching frequency | $f_{\rm sw}$ | 10 kHz |

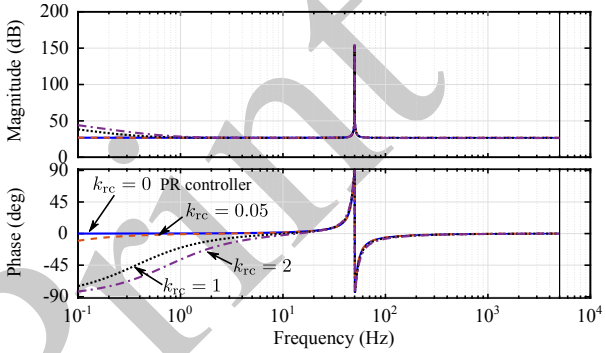


Fig. 8. Bode diagram of the "general" PI controller ($G_{\rm PIR}(z)$) with different repetitive control gains $k_{\rm rc}$, where the Tustin transformation was adopted for discretization, and $k_p$ = 22, $k_r$ = 2000.

### C. Parameter Tuning of the Current Controllers

Actually, when combining the RC controller, $G_{\rm crc}(s)$ and the PR controller, $G_{\rm pr}(s)$, the following current controller $G_{\text{G-PI}}(s)$ is valid,

$$G_{\text{G-PI}}(s) = G_{\rm PIR}(s) + \frac{2k_{\rm rc}}{T_0}\sum_{h=2}^{n}\frac{s}{s^2+\omega_0^2} \tag{23}$$

with $G_{\rm PIR}(s) = k_p' + k_i\frac{1}{s} + k_r'\frac{s}{s^2+\omega_0^2}$ and $k_p' = k_p - \frac{k_{\rm rc}}{2}$ , $k_i = \frac{k_{\rm rc}}{T_0}$ , $k_r' = k_r + \frac{2k_{\rm rc}}{T_0}$. The controller $G_{\rm PIR}(s)$ can be taken as a more "general" PI controller. The Bode diagram of this controller with different control gain $k_{\rm rc}$ (typically, $0 < k_{\rm rc} < 2$ as discussed in [19]) is shown in Fig. 8, which verifies that the frequency response of $G_{\rm PIR}(s)$ is similar to that of a PR controller except for the very low frequency (below 10 Hz). As a consequence, it allows designing the PR controller firstly without the plug-in RC controller.

When it comes to the design of the PR controller, the bode diagram of the open-loop system (i.e., $z^{-1}G_{\rm pr}(z)F(z)$) is normally utilized. For such a controller, the basic design requirements are:

- The system cut-off frequency $\omega_c$ should be high enough in order to cover a wide range of resonant frequencies of the RC controller (up to the Nyquist frequency in theory);
- The fundamental resonant control gain $k_r$ should be as high as possible, when considering a good Phase Margin (PM) [26]. Moreover, a large $k_r$ will lead to a wide

Post-Print

frequency band around the fundamental frequency [13], which can tolerate the grid frequency variation impacts to some extent.

On a basis of the above rules, the fundamental-frequency PR controller is designed as

$$G_{\rm pr}(z) = \frac{22.1 - 21.9z^{-2}}{1 - 2z^{-1} + z^{-2}} \tag{24}$$

which ensures that the closed-loop system is stable (only using PR controller). The corresponding PM is 55.2° at $\omega_c = 5930$ rad/s. This cut-off frequency allows compensating up to the 17$^{\rm th}$-order harmonic.

Regarding the tuning of the RC controller, according to (21), if all the roots of the error $e_i(z)$ locate inside the unity circle, the entire current control system will be stable. Substituting (17) into (21) gives the stability criterion of design as

$$|S(z)| = |Q(z) - k_{\rm rc} z^{-1} Q(z) G_{\rm f}(z) F(z)(1 - G_{\rm clPR}(z))| \leq 1 \tag{25}$$

where $\forall z = e^{j\omega t}$ with $0 < \omega < \pi/T_s$ and $G_{\rm f}(z) = z^m$ is the digital form of the phase-lead compensator. Consequently, the following conditions should hold in order to ensure the entire controller stability:

- The closed-loop system $G_{\rm clPR}(z)$ is stable when the PR controller is adopted;
- The control gain $k_{\rm rc}$ and the phase lead compensation number $m$ should fulfill the inequality shown in (25).

Practically, the control gain $k_{\rm rc}$ is selected as $0 < k_{\rm rc} < 2$ and the low-pass filter $Q(z)$ is introduced to enhance the robustness of the controller at the cost of tracking accuracy [19], [59]. As a rule of thumb, the low-pass filter is normally chosen as $Q(z) = \beta z + \alpha + \beta z^{-1}$ with $\alpha + 2\beta = 1$ and $\alpha$, $\beta > 0$. Due to the model uncertainties or simplified assumptions of the system non-linearity [38], [39], [63], it is relatively difficult to directly design the phase-lead compensator number $m$. Thus, the phase compensation step $m$ is usually determined by experiments. Moreover, preliminary controller parameters can be determined through simulations by means of analyzing the frequency response of the stability function $S(z)$.

In this paper, the RC controller gain has been designed as $k_{\rm rc}$ = 1.8 and the initial phase-lead compensation number has been selected as $m$ = 4. This will result in the designed RC controller as

$$G_{\rm rc}(z) = \frac{0.09z^{-195} + 1.62z^{-196} + 0.09z^{-197}}{1 - 0.05z^{-199} - 0.9z^{-200} - 0.05z^{-201}} \tag{26}$$

where the low-pass filter is designed as $Q(z) = 0.05z + 0.9 + 0.05z^{-1}$ and the sampling frequency $f_s$ = 10 kHz. However, it should be noted that the phase-lead compensator number $m$ should be further determined in the experimental tests.

## IV. Experimental Results

It should be pointed out that the analysis conducted in § II will not be affected significantly by the system configuration as long as the MPPT control is robust. Hence, in order to verify the above discussions and to evaluate the tailor-made current control scheme, experiments have been conducted on two single-phase grid-connected inverter systems: a double-stage inverter system with a PV simulator and a single-stage inverter system. The double-stage system is employed to test the DC-link voltage variations and the grid current quality under different input powers and various power factors. In contrast, the single-stage system is mainly used to evaluate the tailor-made current controller, and to test the harmonic injection under grid voltage sags.

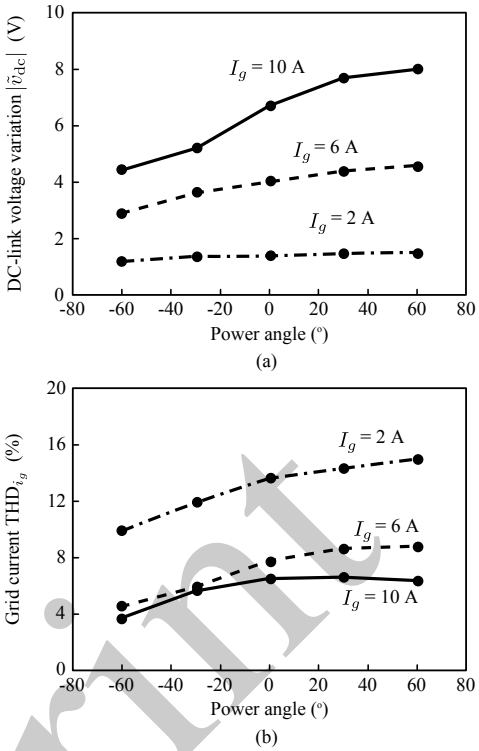


Fig. 9. Experimental results for a single-phase double-stage PV system under different power angles and grid current levels with a proportional resonant controller ($I_g$ - grid current amplitude): (a) DC-link voltage variation amplitude and (b) THD of the injected grid current.

### A. Double-Stage Inverter System

Since the PV panels are highly weather-dependent, resulting in a varying output current level as well as the injected grid current amplitude, a single-phase double-stage grid-connected system [19] is firstly tested under different power angles as well as grid current amplitudes. Notably, the double-stage system has a low power PV simulator and a DC-DC boost converter [13], which is different from the PV system shown in Fig. 1. In this case study, the DC-link voltage is controlled as 100 V with an AC grid of 50 V (root mean square value) and 50 Hz. The DC-DC stage is to ensure the power injection, while the inverter maintains a constant DC-link voltage (i.e., $v_{\rm dc}^*$ = 100 V). The current controller is the same as what is shown in Fig. 5, but only a PR fundamental current controller is adopted. The experimental results are presented in Fig. 9.

It can be observed in Fig. 9(a) that the DC-link voltage variations $|\tilde{v}_{\rm dc}|$ is proportional to the injected grid current level, which is in agreement with the discussions in § II. When the grid current amplitude becomes small, the voltage drop on the

Post-Print

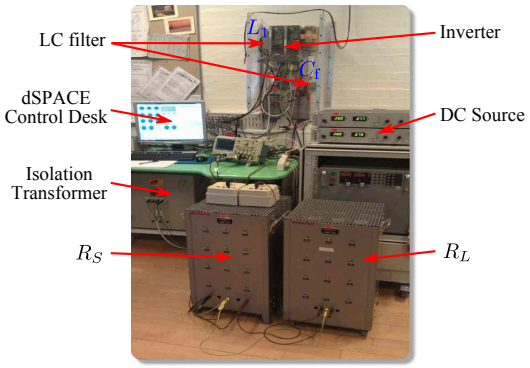


Fig. 10. Experimental setup of a single-phase single-stage grid-connected inverter system.

filter inductor will also become insignificant compared to the grid voltage (i.e., $v_{\text{inv}}^1 \approx v_g^1$; cf., Fig. 3). Hence, according to (11), the DC-link voltage will not change so much, as shown in Fig. 9(a). Moreover, it has also been verified in Fig. 9(b) that the current level will significantly affect the quality of the injected current. Consequently, in the case of weak solar irradiance (i.e., contributing to a low current amplitude), the $\text{THD}_{i_g}$ may increase. Notably, although the DC-link voltage variation is small in that case, the dominant inverter output harmonics $V_{\text{dc}} \sum_{h=2}^{n} d_{\text{pwm}}^h$ remain almost the same and also the fundamental current is smaller, where however the grid voltage distortion exists ($\text{THD}_{v_g} \approx 1\%$). Those result in a poor current quality as shown in Fig. 9(b). Nevertheless, the experimental tests have demonstrated the impacts of the current levels and the power factors on the power quality, and hence a better current controller should be developed to mitigate such harmonics.

### *B. Single-Stage Inverter System*

Fig. 10 shows the single-phase single-stage grid-connected inverter setup, and the system parameters are listed in Table I. In this test rig, a commercial inverter is used as the power conversion stage. The control system is implemented in a DS 1103 dSPACE system referring to Fig. 7. An LC-filter is employed in order to filter out the harmonics at high switching frequencies. A multi-resonant controller consists of the 3rd, 5th and 7th resonant controllers is compared with the tailor-made control solution (i.e., a PR controller with a plug-in RC harmonic compensator). The control gains for the PR controller with the multi-resonant controller are: $k_p$ = 22, $k_r$ = 2000, $k_i^3 = k_i^5$ = 5000 (the 3rd and 5th order), $k_i^7$ = 7000 (the 7th order). The PI controller parameters for the active power are $k_p^p$ = 1.2, $k_i^p$ = 52; while for the reactive power are $k_p^q$ = 1, $k_i^q$=50. The phase-lead compensator number has been determined as $m = 3$. The control gain for the RC controller is $k_{\text{rc}}$ = 1.8.

As discussed in § II, the operational modes have certain impacts on the quality of the injected grid current, which can also be seen in Fig. 9, where both the current THD and the DC-link voltage variations are affected by the power angle. Furthermore, the single-phase single-stage inverter system is tested in different operational modes, and the experimental

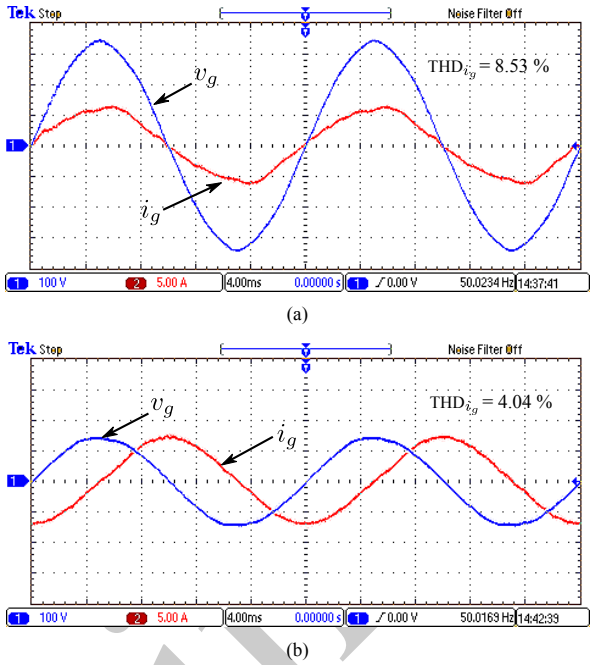


Fig. 11. Experimental results for a single-phase single-stage grid-connected system in different operational modes with a proportional resonant controller (grid voltage $v_g$ [100 V/div], grid current $i_g$ [5 A/div], time [4 ms/div]): (a) normal operation mode and (b) low voltage ride through operation with reactive power injection (voltage sag: 0.45 p.u.).

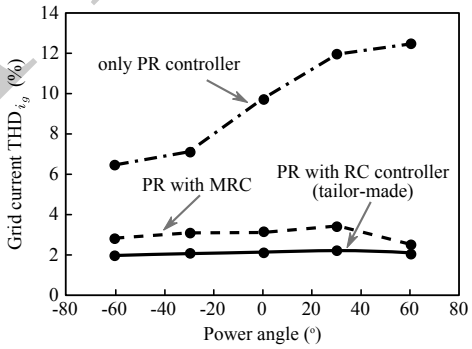


Fig. 12. Grid current THD for a single-phase single-stage grid-connected system under different power angles in the normal operational mode with three current control solutions (grid current amplitude $I_g$ = 6 A, grid voltage amplitude $V_g$ = 325 V).

results are shown in Fig. 11, where a voltage sag (0.45 p.u.) is generated by switching the resistors $R_S$ and $R_L$ and only the fundamental PR controller is adopted as the current controller. During the grid fault, the LVRT control is enabled – the system is injecting reactive power to the grid according to the grid requirements; while the amplitude of the grid current is maintained almost constant in order to prevent the inverter from over-current triggering. In that case, the power factor is not unity. It can observed that, the $\text{THD}_{i_g}$ under the voltage sag is lower. This experimental test has verified that the operation modes of the PV inverters (e.g., fault ride through operation and reactive power injection operation) will affect the quality of the injected current, which is in a close agreement with the discussions in § II.C (cf., (11)). However, in these tests, only the PR controller has been adopted.

Post-Print

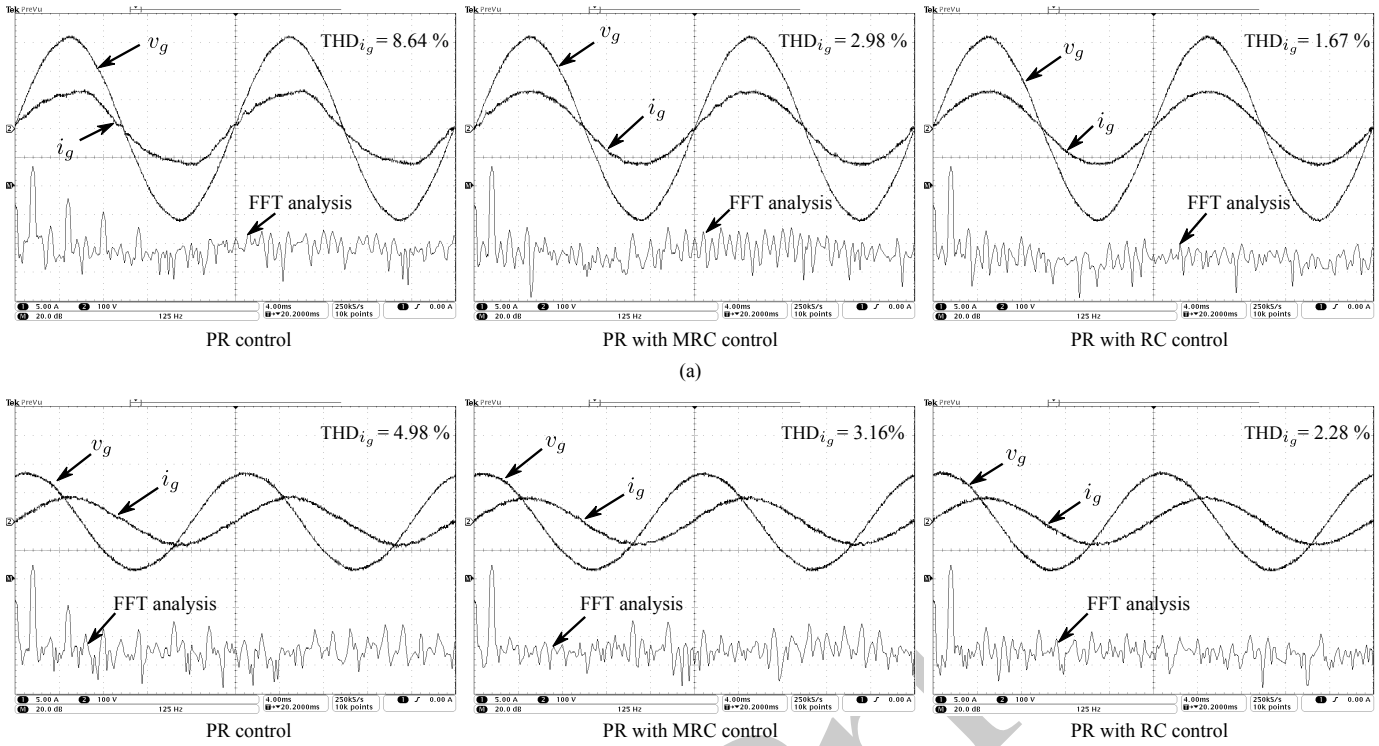


Fig. 13. Experimental results of a single-phase grid-connected system in different operational conditions with various current control methods based on the single-phase $PQ$ theory (CH 1 - grid current $i_g$ [5 A/div], CH 2 - grid voltage $v_g$ [100 V/div], CH M - Fast Fourier Transform (FFT) of the grid current [20 dB/div], time [4 ms/div], FFT frequency [125 Hz/div]): (a) in the normal operation mode and (b) under a grid fault with low voltage ride through control (voltage sag: 0.45 p.u.).

Additionally, in order to verify the effectiveness of the harmonic mitigation by multi-resonant controllers and the tailor-made controller, the single-phase inverter system shown in Fig. 10 has been examined under various power factors. Fig. 12 compares the feed-in grid current THD, when the PR controller, the PR controller with multi-resonant controller, and the tailor-made controller have been adopted. It is observed in Fig. 12 that the tailor-made control method can suppress the harmonics effectively regardless of the power factors. As a consequence, in contrast to the PR controller with multi-resonant controller, the PR controller with a plug-in RC controller offers a better quality of the injected current regardless of the operational modes, according to Fig. 12 and Fig. 13. Since the RC controller can remove high order harmonics effectively, the tailor-made controller can achieve an overall lower current THD as discussed previously. Moreover, the combination of PR and RC controllers brings less computational burden to the digital signal processor in its implementation than what the multiple-paralleled resonant controller does.

Furthermore, the harmonic mitigation capability of the MRC controller and the RC controller is compared as shown in Fig. 14 in both normal operation mode and under a voltage sag. This experimental benchmarking has confirmed the effectiveness of the tailor-made harmonic controller over the MRC controller in terms of an overall low THD. It should also be pointed out that the dynamic of the tailor-made solution may not be as good as that of the PR controller with the multi-resonant controller, since the RC harmonic compensator theoretically acts on all the harmonics below the Nyquist frequency. As shown in Fig. 14, the RC controller can almost maintain lower harmonics in a wide range of frequency (e.g., 50 $\sim$ 2000 Hz). Possibilities to improve the dynamics of the PR controller with a RC harmonic compensator are directed to [34], [59]. Nevertheless, the experimental results have confirmed that the tailor-made control solution provides a promising way to harmonic mitigation in the single-phase grid-connected inverter systems.

## V. Conclusion

This paper has explored the origins for current harmonics injection from single-phase grid-connected inverter systems in different operational modes. The analysis reveals how the injected current distortion varies with the feed-in grid current level (e.g., in different sites and under various environmental conditions for PV systems), the power factor, and the grid voltage level. Accordingly, a tailor-made current control solution has been designed, which has also been tested experimentally on single-phase grid-connected inverters. The test results have verified that the tailor-made current controller (i.e., combining a PR controller and a RC controller) can achieve relatively high control accuracy as well as less complexity. Specifically, this tailor-made solution can suppress the injected harmonics effectively regardless of operation conditions (e.g., power factor, output current level, or grid voltage level). That is to say, the developed current control scheme is not sensitive to

Post-Print

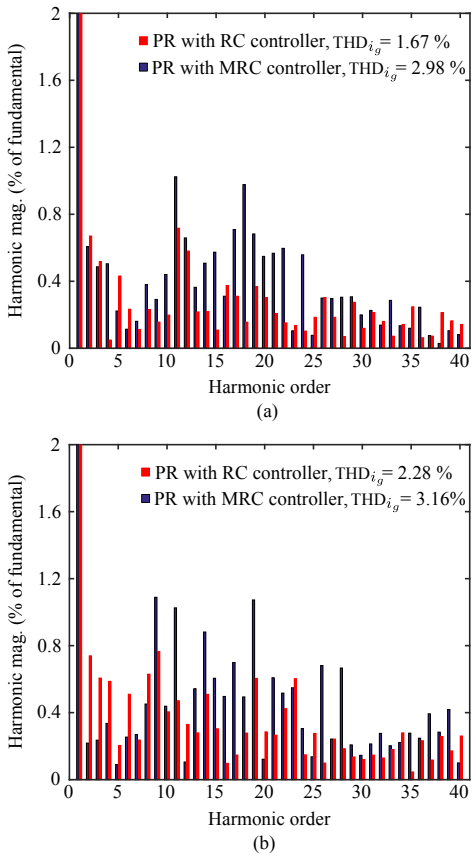


Fig. 14. Harmonic distributions of the grid current for a single-phase single-stage system under different operation modes with a multi-resonant controller and a repetitive controller as the harmonic compensator: (a) in the normal operation mode and (b) in low voltage ride through operation mode (voltage sag: 0.45 p.u.).

the clause changes of grid requirements on current distortion levels of grid-connected single-phase inverters and also the operational conditions. In addition, this tailor-made current controller avoids a redesigning process in different grid-connected applications, where various harmonic requirements will possibly be published.

Furthermore, the future grid-connected PV systems will be more active and more "smart" with ancillary services. In that case, the system will be required to provide reactive current even in the normal operation mode with a maximum power point tracking. Moreover, not only for single-phase PV systems but also for other single-phase DC-AC systems and renewable energy systems is the harmonics injection a big challenge, which thus should be taken care of during the design and operation phases. For example, the single-phase inverters are widely used in fuel cell systems, vehicle-to-grid systems, smart grids, micro-grids, and so on. In those systems, the harmonics will have an impact on the system stability and the operation performance. Fortunately, the tailor-made solution can be extended to those systems without much significant modification.

## REFERENCES

[1] C. Winneker, "Worlds solar photovoltaic capacity passes 100-gigawatt landmark after strong year," [Online], Feb. 2013.

[2] REN21, "Renewables 2015 - Global status report," Tech. Report, Online Available: www.ren21.net, 2015.

[3] Fraunhofer ISE, "Recent facts about phovoltaics in germany," Fraunhofer Inst. Sol. Energy Syst., Freiburg, Germany, Tech. Report, [Online]. Available: www.pv-fakten.de, 19 May 2015.

[4] D. G. Infield, P. Onions, A. D. Simmons, and G. A. Smith, "Power quality from multiple grid-connected single-phase inverters," *IEEE Trans. Power Del.*, vol. 19, no. 4, pp. 1983–1989, Oct. 2004.

[5] P. Acuna, L. Moran, M. Rivera, J. Dixon, and J. Rodriguez, "Improved active power filter performance for renewable power generation systems," *IEEE Trans. Power Electron.*, vol. 29, no. 2, pp. 687–694, Feb. 2014.

[6] J. He, Y. W. Li, F. Blaabjerg, and X. Wang, "Active harmonic filtering using current-controlled, grid-connected DG units with closed-loop power control," *IEEE Trans. Power Electron.*, vol. 29, no. 2, pp. 642–653, Feb. 2014.

[7] P. Gonzalez, E. Romero, V. M. Minambres, M. A. Guerrero, and E. Gonzalez, "Grid-connected pv plants. power quality and technical requirements," in *Proc. of Electric Power Quality Supply Reliability Conf.*, June 2014, pp. 169–176.

[8] "IEEE standard for interconnecting distributed resources with electric power systems," *IEEE Std 1547-2003*, 2003.

[9] "Characteristics of the utility interface for photovoltaic systems," *IEC Std 61727:2004*, Dec. 2004.

[10] "IEEE draft recommended practice for establishing methods and procedures that provide supplemental support for implementation strategies for expanded use of IEEE Standard 1547," *IEEE P1547.8/D8, July 2014*, Sept. 2014.

[11] E.ON Netz, *Grid Code – High and extra high voltage*. E. ON Netz GmbH, Bayreuth, 2006.

[12] Comitato Elettrotecnico Italiano, *CEI 0-21: Reference technical rules for connecting users to the active and passive LV distribution companies of electricity*, 2011.

[13] F. Blaabjerg, R. Teodorescu, M. Liserre, and A. V. Timbus, "Overview of control and grid synchronization for distributed power generation systems," *IEEE Trans. Ind. Electron.*, vol. 53, no. 5, pp. 1398–1409, Oct. 2006.

[14] R. Teodorescu, M. Liserre, and P. Rodriguez, *Grid converters for photovoltaic and wind power systems*. John Wiley & Sons, 2011.

[15] Y. Yang, F. Blaabjerg, and Z. Zou, "Benchmarking of grid fault modes in single-phase grid-connected photovoltaic systems," *IEEE Trans. Ind. Appl.*, vol. 49, no. 5, pp. 2167–2176, Sept.-Oct. 2013.

[16] Z. Shu, S. Xie, and Q. Li, "Single-phase back-to-back converter for active power balancing, reactive power compensation, and harmonic filtering in traction power system," *IEEE Trans. Power Electron.*, vol. 26, no. 2, pp. 334–343, Feb. 2011.

[17] R. Bojoi, L.R. Limongi, D. Roiu, and A. Tenconi, "Enhanced power quality control strategy for single-phase inverters in distributed generation systems," *IEEE Trans. Power Electron.*, vol. 26, no. 3, pp. 798–806, Mar. 2011.

[18] A. Kulkarni and V. John, "Mitigation of lower order harmonics in a grid-connected single-phase PV inverter," *IEEE Trans. Power Electron.*, vol. 28, no. 11, pp. 5024–5037, Nov. 2013.

[19] K. Zhou, Z. Qiu, N.R. Watson, and Y. Liu, "Mechanism and elimination of harmonic current injection from single-phase grid-connected PWM converters," *IET Power Electronics*, vol. 6, no. 1, pp. 88–95, Jan. 2013.

[20] S. Chen, Y. M. Lai, S.-C. Tan, and C. K. Tse, "Analysis and design of repetitive controller for harmonic elimination in PWM voltage source inverter systems," *IET Power Electronics*, vol. 1, no. 4, pp. 497–506, Dec. 2008.

[21] Y. Yang, P. Enjeti, F. Blaabjerg, and H. Wang, "Wide-scale adoption of photovoltaic energy: Grid code modifications are explored in the distribution grid," *IEEE Ind. Appl. Mag.*, vol. 21, no. 5, pp. 21–31, Sept. 2015.

[22] H. Kobayashi, "Fault ride through requirements and measures of distributed PV systems in Japan," in *Proc. PES General Meeting*. IEEE, 2012, pp. 1–6.

[23] R. Teodorescu, F. Blaabjerg, M. Liserre, and P. C. Loh, "Proportional-resonant controllers and filters for grid-connected voltage-source converters," *IEE Proceedings-Electric Power Applications*, vol. 153, no. 5, pp. 750–762, Sept. 2006.

[24] X. Yuan, W. Merk, H. Stemmler, and J. Allmeling, "Stationary-frame generalized integrators for current control of active power filters with zero steady-state error for current harmonics of concern under unbalanced and distorted operating conditions," *IEEE Trans. Ind. Appl.*, vol. 38, no. 2, pp. 523–532, Mar. 2002.

Post-Print

[25] R. Teodorescu, F. Blaabjerg, U. Borup, and M. Liserre, "A new control structure for grid-connected LCL PV inverters with zero steady-state error and selective harmonic compensation," in *Proc. APEC*, vol. 1, 2004, pp. 580–586.

[26] A. G. Yepes, F. D. Freijedo, O. Lopez, and J. Doval-Gandoy, "Analysis and design of resonant current controllers for voltage-source converters by means of nyquist diagrams and sensitivity function," *IEEE Trans. Ind. Electron.*, vol. 58, no. 11, pp. 5231–5250, Nov. 2011.

[27] A.G. Yepes, F.D. Freijedo, O. Lopez, and J. Doval-Gandoy, "High performance digital resonant controllers implemented with two integrators," *IEEE Trans. Power Electron.*, vol. 26, no. 2, pp. 563–576, Feb. 2011.

[28] F. D. Freijedo, A. G. Yepes, J. Malvar, O. Lopez, P. Fernandez-Comesana, A. Vidal, and J. Doval-Gandoy, "Frequency tracking of digital resonant filters for control of power converters connected to public distribution systems," *IET Power Electronics*, vol. 4, no. 4, pp. 454–462, Apr. 2011.

[29] S. A. Khajehoddin, M. Karimi-Ghartemani, P. K. Jain, and A. Bakhshai, "A resonant controller with high structural robustness for fixed-point digital implementations," *IEEE Trans. Power Electron.*, vol. 27, no. 7, pp. 3352–3362, Jul. 2012.

[30] G. Shen, X. Zhu, J. Zhang, and D. Xu, "A new feedback method for PR current control of LCL-filter-based grid-connected inverter," *IEEE Trans. Ind. Electron.*, vol. 57, no. 6, pp. 2033–2041, Jun. 2010.

[31] M. Ciobotaru, R. Teodorescu, and F. Blaabjerg, "Control of single-stage single-phase PV inverter," in *Proc. EPE*. IEEE, 2005, pp. P.1–P.10.

[32] K. Zhou and Y. H. Yang, "Multiple harmonics control of single-phase PWM rectifiers," in *Proc. ISIE*, 2012, pp. 393–396.

[33] K. Zhou, K.-S. Low, Y. Wang, F.-L. Luo, and B. Zhang, "Zero-phase odd-harmonic repetitive controller for a single-phase PWM inverter," *IEEE Trans. Power Electron.*, vol. 21, no. 1, pp. 193–201, Jan. 2006.

[34] K. Zhou, D. Wang, B. Zhang, and Y. Wang, "Plug-in dual-mode-structure repetitive controller for CVCF PWM inverters," *IEEE Trans. Ind. Electron.*, vol. 56, no. 3, pp. 784–791, Mar. 2009.

[35] T. Hornik and Q.-C. Zhong, "A current-control strategy for voltage-source inverters in microgrids based on H-$\infty$ and repetitive control," *IEEE Trans. Power Electron.*, vol. 26, no. 3, pp. 943–952, Mar. 2011.

[36] S. Jiang, D. Cao, Y. Li, J. Liu, and F. Z. Peng, "Low-thd, fast-transient, and cost-effective synchronous-frame repetitive controller for three-phase UPS inverters," *IEEE Trans. Power Electron.*, vol. 27, no. 6, pp. 2994–3005, Jun. 2012.

[37] R. Costa-Castelló, R. Grinó, and E. Fossas, "Odd-harmonic digital repetitive control of a single-phase current active filter," *IEEE Trans. Power Electron.*, vol. 19, no. 4, pp. 1060–1068, Jul. 2004.

[38] Y. H. Yang, K. Zhou, and M. Cheng, "Phase compensation resonant controller for single-phase PWM converters," *IEEE Trans. Ind. Inform*, vol. 9, no. 2, pp. 957–964, May 2012.

[39] Y. H. Yang, K. Zhou, M. Cheng, and B. Zhang, "Phase compensation multiresonant control of CVCF PWM converters," *IEEE Trans. Power Electron.*, vol. 28, no. 8, pp. 3923–3930, Aug. 2013.

[40] W. Lu, K. Zhou, D. Wang, and M. Cheng, "A general parallel structure repetitive control scheme for multiphase DC–AC PWM converters," *IEEE Trans. Power Electron.*, vol. 28, no. 8, pp. 3980–3987, Aug. 2013.

[41] M. Rashed, C. Klumpner, and G. Asher, "Repetitive and resonant control for a single-phase grid-connected hybrid cascaded multilevel converter," *IEEE Trans. Power Electron.*, vol. 28, no. 5, pp. 2224–2234, May 2013.

[42] M. Rashed, C. Klumpner, and G. Asher, "Control scheme for a single phase hybrid multilevel converter using repetitive and resonant control approaches," in *Proc. EPE*. IEEE, 2011, pp. 1–13.

[43] M. Saitou and T. Shimizu, "Generalized theory of instantaneous active and reactive powers in single-phase circuits based on Hilbert transform," in *Proc. PESC*, vol. 3, 2002, pp. 1419–1424.

[44] Y. Yang, F. Blaabjerg, and H. Wang, "Low-voltage ride-through of single-phase transformerless photovoltaic inverters," *IEEE Trans. Ind. Appl.*, vol. 50, no. 3, pp. 1942–1952, May-Jun. 2014.

[45] M. Prodanović, K. De Brabandere, J. Van den Keybus, T. Green, and J. Driesen, "Harmonic and reactive power compensation as ancillary services in inverter-based distributed generation," *IET Gener., Transm. & Distrib.*, vol. 1, no. 3, pp. 432–438, May 2007.

[46] C. H. Benz, W.-T. Franke, and F. W. Fuchs, "Low voltage ride through capability of a 5 kW grid-tied solar inverter," in *Proc. EPE/PEMC*. IEEE, 2010, pp. T12–13–T12–20.

[47] Y. Hanashima and T. Yokoyama, "FRT capability of 100 kHz single phase utility interactive inverter with FPGA based hardware controller," in *Proc. EPE/PEMC*, 2012, pp. LS8b.1–1–LS8b.1–8.

[48] M. Braun, T. Stetz, R. Bründlinger, C. Mayr, K. Ogimoto, H. Hatta, H. Kobayashi, B. Kroposki, B. Mather, M. Coddington *et al.*, "Is the distribution grid ready to accept large-scale photovoltaic deployment? state of the art, progress, and future prospects," *Progr. photovolt., Res. appl.*, vol. 20, no. 6, pp. 681–697, 2012.

[49] M. Braun, "Reactive power supplied by PV inverters–cost benefit analysis," in *Proc. EU PVSEC*, 2007, pp. 3–7.

[50] A. Anurag, Y. Yang, and F. Blaabjerg, "Thermal performance and reliability analysis of single-phase PV inverters with reactive power injection outside feed-in operating hours," *IEEE J. Emerg. Sel. Topics Power Electron.*, vol. 3, no. 4, pp. 870–880, Dec. 2015.

[51] J. W. Smith, W. Sunderman, R. Dugan, and B. Seal, "Smart inverter volt/var control functions for high penetration of PV on distribution systems," in *Proc. of IEEE PES PSCE*, Mar. 2011, pp. 1–6.

[52] A. Chidurala, T. Saha, and N. Mithulananthan, "Harmonic characterization of grid connected PV systems - validation with field measurements," in *Proc. of IEEE PES General Meeting*, Jul. 2015, pp. 1–5.

[53] J. H. R. Enslin and P. J. M. Heskes, "Harmonic interaction between a large number of distributed power inverters and the distribution network," *IEEE Trans. Power Electron.*, vol. 19, no. 6, pp. 1586–1593, Nov. 2004.

[54] N. Mohan, T. M. Undeland, and W. P. Robbins, *Power electronics: converters, applications, and design*. John Wiley & Sons, 2007.

[55] Y. Yang, K. Zhou, H. Wang, and F. Blaabjerg, "Harmonics mitigation of dead time effects in PWM converters using a repetitive controller," in *Proc. of APEC*, Mar. 2015, pp. 1479–1486.

[56] S.-H. Hwang and J.-M. Kim, "Dead time compensation method for voltage-fed PWM inverter," *IEEE Trans. Energy Conversion*, vol. 25, no. 1, pp. 1–10, Mar. 2010.

[57] S. B. Kjaer, J. K. Pedersen, and F. Blaabjerg, "A review of single-phase grid-connected inverters for photovoltaic modules," *IEEE Trans. Ind. Appl.*, vol. 41, no. 5, pp. 1292–1306, Sept. 2005.

[58] L. Hadjidemetriou, E. Kyriakides, Y. Yang, and F. Blaabjerg, "A synchronization method for single-phase grid-tied inverters," *IEEE Trans. Power Electron.*, vol. 31, no. 3, pp. 2139–2149, Mar. 2016.

[59] Y. Yang, K. Zhou, H. Wang, F. Blaabjerg, D. Wang, and B. Zhang, "Frequency adaptive selective harmonic control for grid-connected inverters," *IEEE Trans. Power Electron.*, vol. 30, no. 7, pp. 3912–3924, Jul. 2015.

[60] M. A. Herran, J. R. Fischer, S. A. Gonzalez, M. G. Judewicz, I. Carugati, and D. O. Carrica, "Repetitive control with adaptive sampling frequency for wind power generation systems," *IEEE J. Emerg. Sel. Topics Power Electron.*, vol. 2, no. 1, pp. 58–69, Mar. 2014.

[61] M. Castilla, J. Miret, J. Matas, L. Garcia de Vicuna, and J. M. Guerrero, "Control design guidelines for single-phase grid-connected photovoltaic inverters with damped resonant harmonic compensators," *IEEE Trans. Ind. Electron.*, vol. 56, no. 11, pp. 4492–4501, Nov. 2009.

[62] B. Zhang, D. Wang, K. Zhou, and Y. Wang, "Linear phase lead compensation repetitive control of a CVCF PWM inverter," *IEEE Trans. Ind. Electron.*, vol. 55, no. 4, pp. 1595–1602, Apr. 2008.

[63] Y. F. Wang and Y. W. Li, "A grid fundamental and harmonic component detection method for single-phase systems," *IEEE Trans. Power Electron.*, vol. 28, no. 5, pp. 2204–2213, May 2013.

[64] D. Chen, J. Zhang, and Z. Qian, "An improved repetitive control scheme for grid-connected inverter with frequency-adaptive capability," *IEEE Trans. Ind. Electron.*, vol. 60, no. 2, pp. 814–823, Feb. 2013.

[65] Y. Cho and J.-S. Lai, "Digital plug-in repetitive controller for single-phase bridgeless PFC converters," *IEEE Trans. Power Electron.*, vol. 28, no. 1, pp. 165–175, Jan. 2013.

[66] Q.-C. Zhong and T. Hornik, "Cascaded current–voltage control to improve the power quality for a grid-connected inverter with a local load," *IEEE Trans. Ind. Electron.*, vol. 60, no. 4, pp. 1344–1355, Apr. 2013.

[67] K. Zhang, Y. Kang, J. Xiong, and J. Chen, "Direct repetitive control of SPWM inverter for UPS purpose," *IEEE Trans. Power Electron.*, vol. 18, no. 3, pp. 784–792, May 2003.

[68] Y. Yang, K. Zhou, H. Wang, and F. Blaabjerg, "Harmonics mitigation of dead time effects in PWM converters using a repetitive controller," in *Proc. APEC*, Mar. 2015, pp. 1479–1486.

[69] N. Hoffmann, F. W. Fuchs, and J. Dannehl, "Models and effects of different updating and sampling concepts to the control of grid-connected PWM converters – a study based on discrete time domain analysis," in *Proc. EPE*, Aug. 2011, pp. 1–10.

[70] S. G. Parker, B. P. McGrath, and D. G. Holmes, "Regions of active damping control for LCL filters," *IEEE Trans. Ind. Appl.*, vol. 50, no. 1, pp. 424–432, Jan. 2014.

[71] J. He, Y.W. Li, F. Blaabjerg, and X. Wang, "Active harmonic filtering using current-controlled, grid-connected DG units with closed-loop power control," *IEEE Trans. Power Electron.*, vol. 29, no. 2, pp. 642–653, Feb. 2014.


Post-Print

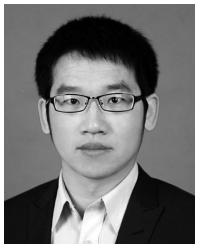

**Yongheng Yang** (S'12 - M'15) received the B.Eng. degree from Northwestern Polytechnical University, Xian, China, in 2009, and the Ph.D. degree from Aalborg University, Aalborg, Denmark, in 2014.

He was a Post-Graduate with Southeast University, Nanjing, China, from 2009 to 2011. In 2013, he was a Visiting Scholar with the Department of Electrical and Computer Engineering, Texas A&M University, College Station, USA. Since 2014, he has been with the Department of Energy Technology, Aalborg University, where he is currently an Assistant Professor. His research interests are focused on grid integration and control of renewable energy systems, harmonics in adjustable speed drives and grid-connected power converters, and the reliability of power electronics.

Dr. Yang is involved in the IEEE Industry Applications Society student activities. He is a Committee Member of the IEEE Power Electronics Society Young Professionals and responsible for the webinar series. He serves as a Guest Associate Editor of the IEEE JOURNAL OF EMERGING AND SELECTED TOPICS IN POWER ELECTRONICS special issue on Power Electronics for Energy Efficient Buildings, and a Session Chair for various technical conferences.

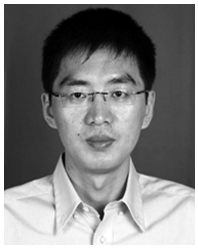

**Keliang Zhou** (M'04 - SM'08) received the B.Sc. degree from the Huazhong University of Science and Technology, Wuhan, China, the M.Eng. degree from Wuhan Transportation University (now the Wuhan University of Technology), Wuhan, and the Ph.D. degree from Nanyang Technological University, Singapore, in 1992, 1995, and 2002.

During 2003-2006, he was a Research Fellow at Nanyang Technological University in Singapore and at Delft University of Technology in the Netherlands, respectively. From 2006 to 2014, he was with Southeast University in China and with the University of Canterbury in New Zealand, respectively. As a Senior Lecturer he joined the School of Engineering at the University of Glasgow in Scotland in 2014. He has authored or coauthored about 100 technical papers and several granted patents in relevant areas. His teaching and research interests include power electronics and electric drives, renewable energy generation, control theory and applications, and microgrid technology.

**Frede Blaabjerg** (S'86 - M'88 - SM'97 - F'03) was with ABB-Scandia, Randers, Denmark, from 1987 to 1988. From 1988 to 1992, he was a Ph.D. Student with Aalborg University, Aalborg, Denmark. He became an Assistant Professor in 1992, an Associate Professor in 1996, and a Full Professor of power electronics and drives in 1998. His current research interests include power electronics and its applications such as in wind turbines, photovoltaic (PV) systems, reliability, harmonics and adjustable speed drives.

Prof. Blaabjerg has received 15 IEEE Prize Paper Awards, the IEEE PELS Distinguished Service Award in 2009, the EPE-PEMC Council Award in 2010, the IEEE William E. Newell Power Electronics Award 2014 and the Villum Kann Rasmussen Research Award 2014. He was an Editor-in-Chief of the IEEE TRANSACTIONS ON POWER ELECTRONICS from 2006 to 2012. He has been Distinguished Lecturer for the IEEE Power Electronics Society from 2005 to 2007 and for the IEEE Industry Applications Society from 2010 to 2011. He is nominated in 2014 by Thomson Reuters to be between the most 250 cited researchers in Engineering in the world.